Functional brain mapping by blood oxygenation level-dependent contrast magnetic resonance imaging
A comparison of signal characteristics with a biophysical model

S. Ogawa,* R. S. Menon,‡ D. W. Tank,* S.-G. Kim,‡ H. Merkle,‡ J. M. Ellermann,‡ and K. Ugurbil‡

*Biological Computation Research Department, AT&T Bell Laboratories, Murray Hill, New Jersey 07974 USA; and
‡Center for Magnetic Resonance Research, University of Minnesota Medical School, Minneapolis, Minnesota 55455 USA

ABSTRACT It recently has been demonstrated that magnetic resonance imaging can be used to map changes in brain hemodynamics produced by human mental operations. One method under development relies on blood oxygenation level-dependent (BOLD) contrast: a change in the signal strength of brain water protons produced by the paramagnetic effects of venous blood deoxyhemoglobin. Here we discuss the basic quantitative features of the observed BOLD-based signal changes, including the signal amplitude and its magnetic field dependence and dynamic effects such as a pronounced oscillatory pattern that is induced in the signal from primary visual cortex during photic stimulation experiments. The observed features are compared with the results of Monte Carlo simulations of water proton intravoxel phase dispersion produced by local field gradients generated by paramagnetic deoxyhemoglobin in nearby venous blood vessels. The simulations suggest that the effect of water molecule diffusion is strong for the case of blood capillaries, but, for larger venous blood vessels, water diffusion is not an important determinant of deoxyhemoglobin-induced signal dephasing. We provide an expression for the apparent in-plane relaxation rate constant (R_2^*) in terms of the main magnetic field strength, the degree of the oxygenation of the venous blood, the venous blood volume fraction in the tissue, and the size of the blood vessel.

INTRODUCTION

Functional brain mapping in humans using magnetic resonance imaging (MRI) of intrinsic signal changes (1-3) recently has been demonstrated. In general, MRI-based brain mapping relies on neural activity-induced localized changes in the chemical or magnetic environment. Localized physiological changes have long been observed and are the basis for other brain mapping methods, including positron emission tomography (PET) (4, 5) and intrinsic signal optical reflection imaging (6-8). One of the major responses that accompanies changes in neural activity is a localized change in cerebral hemodynamics, i.e., changes in cerebral blood flow (CBF), cerebral blood volume (CBV), and blood oxygenation. For example, PET experiments demonstrate that sensory stimulation provides increases in CBF and CBV in the corresponding primary sensory cortex.

Current MRI brain mapping methods also measure these changes in cerebral hemodynamics. Different imaging strategies are used to emphasize one or more of several different physical phenomena that accompany hemodynamic changes. For example, a change in the flow of new blood water into an image slice can be measured directly as a T_1^* rate constant change. Similarly, when blood water occupies a large fraction of total water in an image voxel, an increase of the blood water signal due to an oxygenation level-dependent change in T_2 relaxation (9) could be measured. Gradient-echo MRI emphasizes local susceptibility changes produced by changes in the concentration of deoxyhemoglobin in venous blood vessels (a T_2^* rate constant change [10]). This latter effect is called blood oxygenation level-dependent (BOLD) (11) contrast and is, at present, the most widely studied MRI functional imaging method.

Some of the basic biophysical properties of hemoglobin and susceptibility effects in nuclear magnetic reso-nance that are responsible for BOLD contrast were discovered in pioneering experiments several decades ago. Pauling and Coryell (12) first showed that deoxyhemoglobin is paramagnetic and that the magnetic property of blood depends on the degree of blood oxygenation and therefore on the physiology. By analyzing the nuclear magnetic resonance signal from coaxial tubes containing liquids that differed in their magnetic susceptibility and placed perpendicular to the magnetic field, McConnell and his colleagues (13) showed the existence of a field inhomogeneity in the annular compartment of the outer cylinder. In BOLD imaging, the paramagnetic property of blood produces bulk susceptibility difference between a blood vessel and the surrounding tissue, producing resonance frequency shifts in extra-vessel molecules.

In the vicinity of capillaries and venules, local magnetic field distortions are generated by the presence of paramagnetic deoxyhemoglobin in the blood. These local fields cause intravoxel phase dispersion in water protons, and the resultant image signal becomes weaker than that without the phase dispersion. This effect is pronounced in gradient echo images where the intravoxel phase dispersion directly contributes to increase the apparent transverse relaxation (the rate constant R_2^* or $1/T_2^*$) (10, 11). This additional R_2^* depends on the level of venous blood oxygenation. Since many water molecules are altered by the change in hemoglobin, a form of signal amplification occurs, and water proton functional MRI can depict, at high spatial resolution, the area of neural activation. BOLD is a completely noninvasive method of functional brain mapping, and maps easily can be registered with conventional anatomical MRI brain images.

Although the measurement of the induced signal change is rather simple, requiring only a standard gra-

dient echo pulse sequence taken rapidly enough to minimize motion artifacts, a quantitative understanding of the magnitude of the observed signal changes is presently lacking. In this study we discuss the quantitative characteristics of the signal change observed during photic stimulation experiments. Based on a rather simple model, we also performed Monte Carlo simulations of phase dispersion of water molecules in the vicinity of blood vessels. The goal of these simulations was to determine the basic features of the dependence of BOLD contrast on hemodynamic variables.

The modeling and simulations are similar to those used by Fisel et al. (14) in a theoretical study of magnetic resonance contrast induced by exogenous vascular contrast agents. In general, for strong susceptibility effects of long-range diffusion, it is important to take into account an anatomically correct detailed vascular geometry (15). However, the magnitude of the magnetic susceptibility effects in BOLD contrast is more than an order of magnitude smaller than that produced by exogenous vascular contrast agents. In this low susceptibility effect range, the overlap of the susceptibility-generated fields produced by neighboring blood vessels is minimal. In addition, the diffusion of water molecules during the image echo time of experimental interest is small compared with the average intervessel distance. Therefore, we did not use an anatomically detailed vascular model to understand basic principles of the dependence of BOLD contrast on hemodynamic variables. Rather, we calculated the signal from a small compartment that contained one vessel, and an estimate of the signal intensity from an image voxel was calculated by appropriate averaging over vessel orientations.

MATERIALS AND METHODS

BOLD imaging

MRI measurements were made using a 4T whole body system with actively shielded gradient coils (SISCO, Sunnyvale, CA, and Siemens, Erlangen, Germany) under conditions similar to those previously described (1). Approval for human experiments was obtained from the institutional review board of the University of Minnesota Medical School. A quadrature-driven surface coil was used for radio frequency power transmission and signal reception. Inversion recovery T_1-weighted images were taken for anatomical information (1). Consecutive gradient echo images (54 images in a series) were obtained by using a modified fast low angle shot sequence (echo time = 40 ms, repetition time = 45 ms, 64 phase encoding steps and 128 complex readout points) with an interimaging period of 2 s. The total elapsed time between the start of each image acquisition period was 5 s. An oblique slice that contained the primary visual cortex along the calcarine fissure was chosen from a sagittal slice anatomical image of the subject.

Visual stimulation was provided by a pair of goggles containing light-emitting diode arrays (model S10VS goggles; Grass Co., Quincy, MA). The protocol used in the present report was an image sequence containing 15 dark, 10 stimulus, 10 dark, 10 stimulus, 10 dark images. The first image was discarded because of the non-steady-state condition of the magnetization.

Monte Carlo simulation of intravoxel dephasing

The basic principle of BOLD contrast is an intravoxel phase dispersion of water proton spins due to local magnetic fields produced by nearby deoxyhemoglobin-containing blood vessels. To model the effect, we numerically calculated the expected signal attenuation due to the phase dispersion for a voxel containing an assembly of blood vessels. An image voxel was considered to be composed of a collection of smaller cubic compartments. Each small compartment contained a single blood vessel, modeled as a straight blood-containing cylinder running through the center of two parallel surfaces on opposite sides of the cube. The size of the compartment was chosen for a specific cylinder radius (a) and blood volume fraction (b), such that the edge dimension (L) of the cube was determined from the relation:

$$b = \frac{V_{cylinder}}{V_{compartment}} = \frac{\pi a^2 L}{L^3}.$$

For vessels oriented at an angle θ to the applied magnetic field, the cubic compartment rotated with the vessel. Thus, the voxel was considered to consist of a set of oriented compartments, each containing a single blood vessel. The total volume of the set of cubic compartments equaled the voxel volume.

Our general procedure was to determine the signal attenuation factors produced in a cube of this size for each θ in a set of values that spanned the range $[0, \pi]$, corresponding to a uniform orientational distribution of vessels in the larger image voxel ($\sim$1.6 million cubes in a voxel of $1.6 \times 3.3 \times 10$ mm^3). The appropriate total signal attenuation for the voxel was then calculated by appropriate averaging (see below) over these orientations.

The signal dephasing for water molecules in each small cube depends on the local magnetic field variation, which in turn depends on the orientation of the vessel and the volume susceptibility difference ($\Delta\chi$) between the blood in the cylinder and the surrounding space (tissue). The spatial dependence of the induced magnetic field, ω_B, relative to the field far away from the vessel, given as the component along the direction of the applied magnetic field, is expressed by (16):

outside cylinder

$$\omega_B = 2\pi\Delta\chi(1 - Y)\omega_0 \sin^2(\theta)\left(\frac{a}{r}\right)^2 \cos(2\varphi), \qquad (1)$$

inside cylinder

$$\omega_B = 2\pi\Delta\chi(1 - Y)\omega_0(3\cos^2(\theta) - 1)/3. \qquad (2)$$

In the above equations, ω_0 is the main magnetic field (B_0) in terms of angular frequency, $(1 - Y)$ is the degree of deoxygenation of the blood, θ is the angle between the applied magnetic field B_0 and the cylinder axis, a is the cylinder radius, r is the distance between the point of interest and the center of the cylinder cross-section in the plane normal to the cylinder, and φ is the angle between this vector (r) and the component of B_0 in the plane. The susceptibility difference between 100% deoxy blood and 100% oxygenated blood (which is essentially the same as tissue) was taken as 0.1 ppm (17). The formula in Eq. 1 assumes the field dependence that would be produced by a long, straight blood vessel running through the compartment. We used this assumption since the largest compartment size used in our simulations was less than one third the typical length of an unbranched segment of brain capillary (18).

To numerically compute the dephasing, the cube interior was discretized into $16 \times 16 \times 16 = 4,096$ initial starting lattice points, and a three-dimensional random walk $r(t)$ (not discretized to a lattice) for a water molecule was generated from each site. The random walk was calculated using the method of Einstein. At each time step τ (100 μs or shorter), the water molecule moved in a random direction a short distance $(6D\tau)^{1/2}$, where $D = 1.0 \times 10^{-5}$ cm^2/s was the diffusion

coefficient for water. Because of the redundancy in the 16 positions along the direction of the vessel axis (and the equivalence of the fields generated by θ and $\pi - \theta$), there were effectively 32 different random walks generated from each nonequivalent starting point.

In most of the cases we allowed the random walk to traverse outside the boundaries of the cube. We refer to this condition as the free diffusion model. To investigate the importance of edge effects, in some cases (noted in the text), the walls of the cube compartment were impenetrable barriers. We refer to this condition as the constrained diffusion model. In all cases, the walls of the blood vessel cylinder at the center of the cell were considered as impenetrable barriers.

Each walk lasted for the echo time t_e, and the accumulated phase ϕ along the path, produced by the field distortion, was calculated from numerical integration of:

$$\phi(\theta) = \int_0^{t_e} \{ \omega_B(\theta, \mathbf{r}(t)) + \omega_h(\mathbf{r}(t)) \} \, dt, \qquad (3)$$

where ω_h represents static field variations in the voxel other than ω_B. In the present study, ω_h is taken to be uncorrelated with ω_B and therefore set to zero in the calculation (19). Eq. 3 for the accumulated phase corresponds to gradient echo image acquisition. In some cases (noted in the text) the sign of the accumulated phase was reversed at $t_e/2$ to correspond to a spin-echo image acquisition.

Each random walk produced an accumulated phase and a corresponding phase factor $e^{(i\phi)}$. From the collection of phase factors produced by the set of random walks, the attenuated signal in a voxel relative to the signal without the phase dispersion ($\phi_0 = 0$) was calculated as:

$$S(\theta)e^{i\Phi(\theta)} = \frac{\displaystyle\sum_{\text{paths}} e^{i\phi(\text{path},\theta)}}{\displaystyle\sum_{\text{paths}} e^{i\phi_0}} \approx S(\theta).$$

The resultant signal magnitude and its residual phase were $S(\theta)$ and $\Phi(\theta)$. Because of the spatial symmetry of ω_B, the residual phase $\Phi(\theta)$ is always essentially zero for the tissue water resonance.

$S(\theta)$ was computed for 16 vessel orientations between $\theta = 0$ and π. The voxel signal attenuation was then computed from the orientational average:

$$S_{\text{voxel}} = \frac{\displaystyle\sum_{\theta} S(\theta) \sin(\theta)}{\displaystyle\sum_{\theta} \sin(\theta)}, \qquad (4)$$

where $\sin(\theta)$ represents the vessel orientation density at angle θ for an isotropic distribution.

In Eq. 4, S_{voxel} is a function of the echo time t_e. For several parameter choices, numerical simulations for increasing t_e demonstrated that the computed signal attenuation followed a surprisingly simple exponential decay $S_{\text{voxel}} = S^0_{\text{voxel}} e(-R_2^* t_e)$ in the range of t_e between 10 and 65 ms. In the figures, we have therefore expressed the BOLD produced attenuation as an effective transverse relaxation rate constant R_2^*. In the majority of parameter conditions, the full decay curve was not calculated. Rather, S_{voxel} was calculated for two echo times t_e1 and t_e2, and R_2^* was determined from the relation:

$$R_2^* = \frac{-\ln\left(\dfrac{S_{\text{voxel}}(t_e^1)}{S_{\text{voxel}}(t_e^2)}\right)}{(t_e^2 - t_e^1)}.$$

Except where noted, $t_e^1 = 15$ ms and $t_e^2 = 40$ ms.

Fisel et al. (14) have reported simulations of signal attenuations for susceptibility gradient–based dephasing for the case relevant to the presence of strong exogenous paramagnetic contrast agent in blood. Our procedure is different from theirs in a few significant ways: (a) we deal with much smaller susceptibility differences, (b) the frequency shift to calculate the phase accumulation is the local field component along the main field not along the field normal to the cylinder, (c) the orientational average among various values of θ is made by averaging of the phase factors $e^{i\phi}$ and not with an orientational average of the accumulated phase ϕ itself, and (d) the water diffusion constant D is taken to be the value measured in brain tissue 10^{-5} cm^2/s by Le Bihan and Turner (20) (2.5-fold smaller than that used in Fisel et al. [14]).

In the results reported here, we ignored the contribution from the small volume of blood water. The line-broadening factor during the acquisition period was also ignored.

RESULTS

An example of a functional brain map produced by gradient echo MRI imaging of BOLD contrast is shown in Fig. 1. This particular experiment examined activation of human primary visual cortex produced by a patterned flash visual stimulation. The imaging conditions are summarized in the Methods section and are similar to those reported previously (1). The image on the left is an inversion-recovery T_1-weighted anatomical image taken in an oblique slice along the calcarine fissure in the occipital lobe. This fissure is the known anatomical location of human primary visual cortex. The distinction between gray matter and white matter is clearly evident. White matter has high intensity and thus appears white in the image because of the faster recovery from inversion. The image at the right is a superposition of the anatomical image at the left and a functional map produced from the difference between gradient echo images taken during visual stimulation and those taken during nonstimulation periods. The activated areas correspond to increases in the gradient echo image signal strength. The superimposed map on the anatomical image clearly shows that the strong changes induced by stimulation were confined to gray matter regions.

The magnitude of the fractional signal change ([stimulation − no stimulation]/no stimulation) produced by the patterned flash visual stimulation varied with the location in the image. The largest changes were typically between 5 and 20%. Signal changes of this magnitude have been observed at 4 T for other sensory and motor activation experiments.

The functional image shown in Fig. 1 was computed by subtracting an averaged image intensity computed from the images taken during no visual stimulation from an average of two consecutive images taken during the 50-s stimulation period. Functional images computed during other segments of the stimulation had slightly different patterns: the location of the strongest changes moved around on the image. The reason for this is apparent in the time course of the signal intensity, which is shown in Fig. 2 for three fixed image locations. The base line fluctuations appears uncorrelated in different spatial locations, but the induced signal change shows a time-dependent pattern during stimulation. The pattern differed among locations, but at each location the same pattern was observed in the second period of stimulation

FIGURE 1   Functional brain mapping in human primary visual cortex. The left image is a T_1 weighted inversion recovery anatomical image of an oblique slice from the occipital lobe that contains the calcarine fissure. The right image is a superposition of the anatomical image at the left and the difference image produced from gradient echo images. The differences were calculated by averaging the local signal intensity for the period of photic stimulation and subtracting the corresponding average calculated for the period without stimulation. Areas with large signal changes are indicated.

as was seen in the first. Therefore, the oscillatory signal dynamics induced by the visual stimulation was not due to the base line fluctuations.

We would like to quantitatively understand the phenomenon demonstrated in Figs. 1 and 2. The functional brain image signal observed in simple gradient echo MR images has been attributed mainly to the change in the venous blood oxygenation level due to neurally activated regional CBF changes. An altered venous blood oxygenation should produce a change in BOLD contrast. The basic principle of BOLD contrast is an intravoxel dephasing of water proton spins due to local field gradients produced by nearby blood vessels containing deoxyhemoglobin. To model the BOLD effect, we numerically calculated the expected signal attenuation due to dephasing for a voxel containing an assembly of blood vessels in the parameter range relevant to normal physiological condition. Details of the numerical simulation are given in Methods. Our emphasis was on examining the dependence of water molecule diffusion on the signal attenuation. The calculations are for tissue water and do not include the blood water contribution. When the blood volume fraction (b) is small, the latter is very small.

Figure 3 shows the computed relaxation rate constant $R_2^* = 1/T_2^*$ as a function of the susceptibility induced frequency shift (ν) at the blood vessel surface, defined as:

$$\nu = \Delta\chi(1 - Y)\omega_0.$$

(For purposes of comparison, a blood oxygenation level of $Y = 0.60$ produces a frequency shift $\nu = 43$ Hz at a magnetic field of 4 T.) The radius of the blood vessel was 2.5 μm, and the value of b was fixed as 0.02. As shown in the top curve, with no water diffusion ($D = 0$), R_2^* is a linear function of ν. Since the field distortion only depends on the quantity (r/a), one expects that this R_2^* rate is independent of cylinder radius as long as the

blood volume fraction (b) is kept constant. This was confirmed in numerical simulations (data not shown).

In contrast to the $D = 0$ (static) case, when water molecules diffused at the rate measured in human brain ($D = 10^{-5}$ cm^2/s), the dependence of R_2^* on ν was approximately quadratic for a small vessel (2.5-μm radius; $b = 0.02$) for $\nu < 50$ Hz, becoming linear at larger ν. The calculated values of R_2^* depended slightly on the form of diffusion used in the numerical simulation. At high ν, R_2^* was increased slightly more in the constrained diffusion model (filled circles) relative to that observed with the free diffusion model (solid line). Also in contrast to the static case, the amount of signal attenuation depended on the vessel radius for small vessels. This is shown in Fig. 4, where R_2^* is plotted against the vessel radius. The blood volume fraction was held constant at $b = 0.02$, and the results are shown for several different susceptibility-induced frequency shifts ν. Below 8 μm, there is a strong dependence of the attenuation on the vessel radius. But for larger radii, the diffusion process is not as important, and the rate increases to a constant value similar to that observed for the $D = 0$ case.

Because of the qualitatively different effects observed for vessels < 8-μm radius versus those that are larger, it is convenient to consider the attenuation observed in a complex tissue as being contributed by the effects of two different populations of vessels. Then the tissue R_2^* can be approximated by a sum of two terms, one for large vessels (>8-μm radius) and another for small vessels (<8-μm). It may be appropriate to consider the small vessel population as the capillaries and the larger vessel population as being comprised of the venules and veins.

In general, BOLD signal attenuation is strongly dependent on the blood volume. In addition, changes in blood volume accompany changes in neural activity. We therefore tried to characterize the functional dependence of R_2^* on changes in blood volume. In the case of a large vessel or in the case of no diffusion ($D = 0$), when one
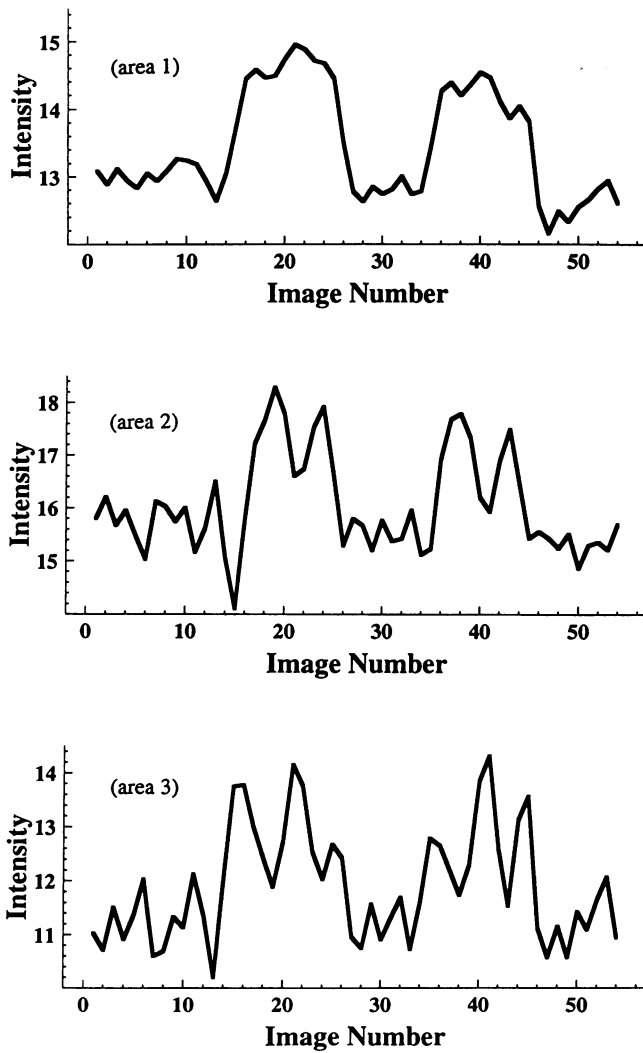
FIGURE 2 The time course of gradient echo image signal intensity at three locations. Image acquisition rate was 5 s per image and photic stimulation was given during image 15 through 24 and image 35 through 44. The time course was temporally averaged with a two-point Gaussian filter to reduce high frequency noise.

$$\frac{\Delta R_2^*}{\Delta b^\gamma} \approx \text{constant}.$$

For the free diffusion model (see Methods), the value of γ was 0.5. This square root dependence was slightly altered in the constrained diffusion model, where the data was better approximated $\gamma = 1$, i.e., by R_2^* varying linearly with b (data not shown).

There are two different models that have been used to describe the changes in microvasculature that accompany changes in CBV. One is called the recruitment model. In this model, capillaries are considered to have two functional states: inactive and active. In the inactive state, blood cells do not pass, although plasma may, through the capillary. An increase in the effective CBV is accompanied by an increased fraction p of active capillaries. Recruitment was modeled in our simulations by considering the population of compartments that comprise an image voxel as containing either an active or inactive vessel. An inactive vessel has $\Delta\chi = 0$. The fraction p represents the fraction of active vessels in the voxel. Changes in CBV thus represent changes in the active vessel population with no change in blood vessel geome-
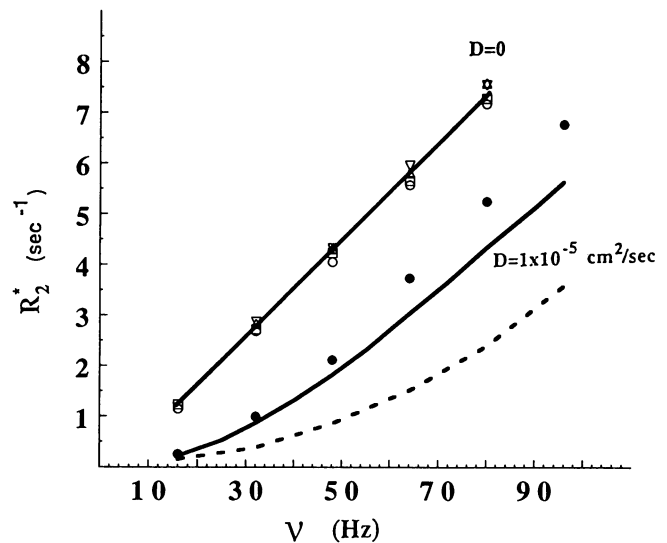

FIGURE 3 The susceptibility-induced R_2^* calculated for a voxel containing 2.5-μm radius blood vessels in the presence and absence of water diffusion. The top straight line is for the case $D = 0$ and a blood volume fraction $b = 0.02$. The rates represented by the open symbols along this line where also calculated for $D = 0$, but for $b = 0.03, 0.04$, and 0.05 and then divided by $b/0.02$ to show a linear dependence of R_2^* on b. The solid middle line for $D = 10^{-5}$ cm^2/s and $b = 0.02$ was calculated using the free diffusion model, whereas the filled circle points were computed with identical parameters but for the constrained diffusion model. The broken line is for the case where diffusion is present but the blood oxygenation level has an exponential variation from 1.0 to Y along the path of the capillary. The plot is made in terms of the shift frequency ν that encompasses the physiological range of venous blood oxygenation level at 4 T field ($\nu = 107.4$ Hz at $Y = 0$).

fixes the radii of the vessel constant and varies the blood volume fraction b, the rate constant R_2^* in the voxel is a linear function of b. This is shown by the clustering of different shaped points in the upper curve of Fig. 3. Each point refers to a different blood volume fraction but was normalized to the case of $b = 0.02$ by dividing the computed R_2^* by the factor ($b/0.02$). The fact that the points for each value of ν can be superimposed implies that R_2^* is a linear function of b.

For smaller sized blood vessels, fixing the blood vessel radius and increasing the blood volume fraction, i.e., reducing the size of the cubic compartment or, equivalently, reducing the average intercapillary distance, increases R_2^*. Our numerical simulations (data not shown) show that the change in R_2^* produced by a change in b can be described as:
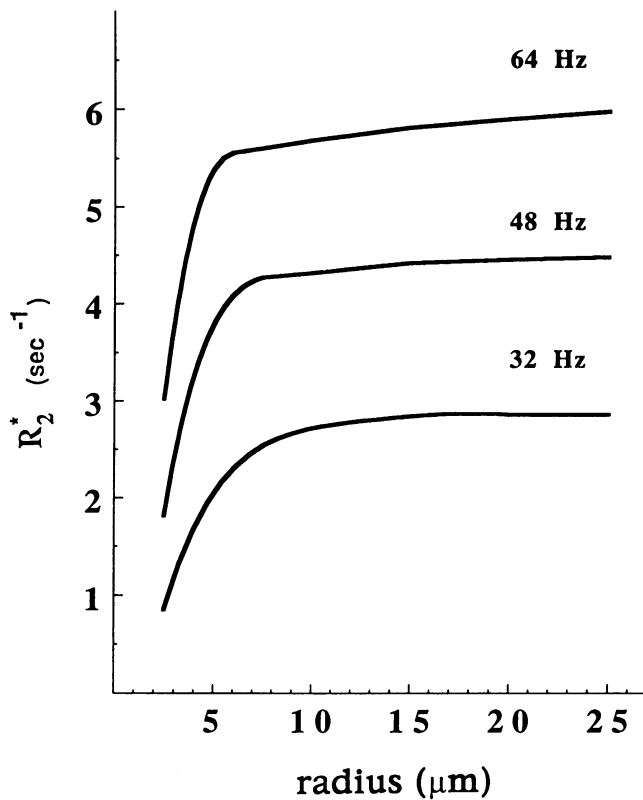
FIGURE 4   The susceptibility induced R_2^* in the presence of water diffusion plotted as a function of cylinder radius. Plots are shown at several values of frequency shifts ($b = 0.02$, echo time $t_e = 40$ ms).

try within the voxel. As shown in Fig. 5 A, numerical simulations for small sized vessels (2.5-μm radius) demonstrated that R_2^* is proportional to p.

An alternative model of hemodynamic change is vessel dilation, where the radius of the vessel changes in order to produce a change in blood fraction b without changing the intervessel distance or the size of the compartment. Dilation was modeled by keeping the cubic compartment size constant and changing the vessel radius to produce a change in b. As shown in Fig. 5 B, numerical simulations demonstrate that the dependence of R_2^* on blood fraction b is approximately linear for small vessel sizes.

Given these results on the frequency, size, and fractional blood volume dependence of R_2^* produced by small vessels and large vessels, we can provide an approximate expression for intravoxel R_2^* in the presence of water diffusion:

$$R_2^* = \begin{cases} \alpha v b_1 & \text{large vessels} \\ \beta v^2 (b_s)^\gamma p & \text{small vessels} \end{cases} \qquad (5)$$

where b_1 and b_s are the blood volume fractions for large vessels (venules and larger veins) and for small vessels (capillary-sized vessels), respectively. The first term in Eq. 5 for large vessels is linear in the shift frequency v, and the value of α that best fit our simulation results was $\alpha = 4.3 \pm 0.3$. The second term for small vessels is quadratic in the shift frequency v, and for both the dilation model and the recruitment model our simulation for capillary-sized vessels could be fit well by $\gamma = 1.0$ and $\beta = 0.04 \pm 0.01$. When referring to the recruitment model, p is the fraction of active vessels and b_s is the maximum blood volume fraction if all vessels were active ($p = 1$). In the dilation model, $p = 1.0$ and b_s is the blood volume fraction. These coefficients refer to the parameter range of echo time below 50 ms and the frequency (v) lower
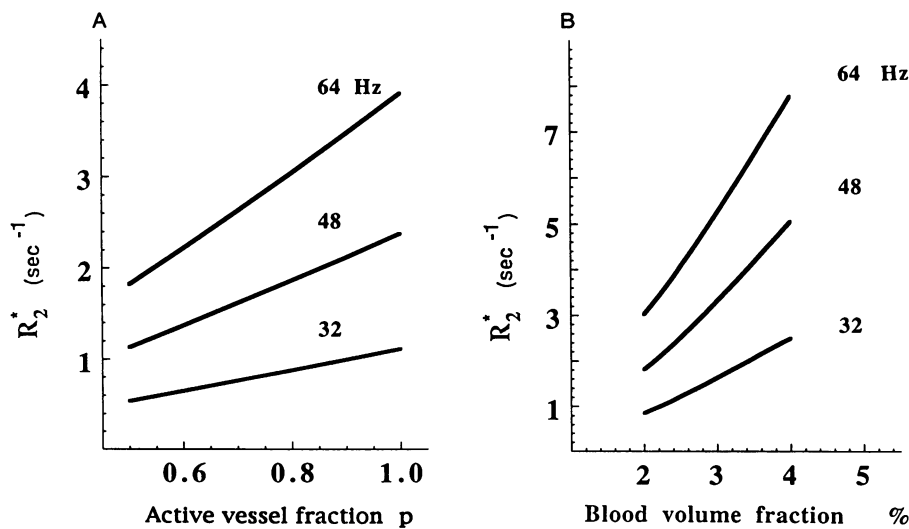

FIGURE 5   (A) The dependence of R_2^* on the active vessel fraction p in the capillary recruitment model ($b = 0.03$, vessel radius of 2.5 μm). (B) The dependence of R_2^* on blood volume fraction for a constant population of blood vessels. The intercapillary distance was held constant at 31 μm, equivalent to that used for $b = 0.02$ with a cylinder radius of 2.5 μm. Increases in blood volume are produced by increases in vessel radius. This corresponds to the dilation model. The values of the shift frequency v are indicated in the figures.
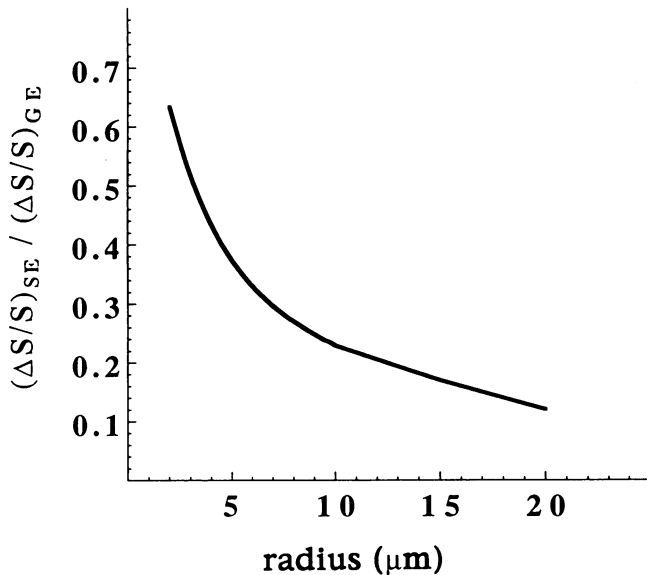
FIGURE 6   The ratio of $\Delta S/S$ for spin echo to $\Delta S/S$ for gradient echo image acquisition as a function of cylinder radius ($b = 0.02$, echo time $t_e = 40$ ms; $\nu = 40$ Hz).

than 70 Hz. For a voxel containing both large and small vessels, the contributions from the two expressions in Eq. 5 must be appropriately summed.

For a physiologically realistic comparison of the contributions from capillaries and noncapillaries, there is another complexity to deal with. In a capillary, the blood oxygenation changes along the path to reach the venule. Therefore, the susceptibility of the capillary blood is effectively lower than that of venous blood. Estimates of R_2^* of a capillary bed in this circumstance were made in a case of 4 T field, assuming the blood oxygenation level changes exponentially from 1.0 at the arterial side to Y at the venule side. In Fig. 3, R_2^* for this situation as a function of the frequency shift of the corresponding venous blood is plotted as the broken line. The relationship is still quadratic, and in the physiological range ($\nu < 60$ Hz), the curve can be made to correspond to the original curve in Fig. 3 (solid line for $D = 10^{-5}$ cm^2/s) by substituting ν with 0.7ν, i.e., an effectively reduced frequency shift. If one uses the average oxygenation level of the capillary blood for Y in the second term of Eq. 5, then this correction factor is 0.5 instead of 0.7.

Our numerical results also can be used to estimate the fractional signal changes expected in spin echo versus gradient echo images. In general, one expects that the diffusion-independent dephasing effects observed at large radii will be absent in spin echo images but not in gradient echo images. For small vessels, averaging the field by diffusion is extensive; therefore, the difference between gradient echo and spin echo imaging is small. These qualitative predictions are evident in Fig. 6, where the ratio of the fractional signal change ($\Delta S/S$) due to the change in the shift frequency around $\nu = 40$ Hz with

$b = 0.02$ is plotted as a function of blood vessel radius. The spin echo/gradient echo ratio for capillaries (radius 2.5 μm) is 0.6 and very similar, regardless of whether or not one assumes an exponential drop in Y with distance along the capillary length. It is also insensitive to the field strength between 4 T and 1.5 T. Our calculated ratio is substantially larger than the value of approximately one fourth at 1.5 T field reported by Bandettini et al. (21) for the fractional signal changes observed in a motor cortex activation experiment. This may indicate that at the lower field (1.5 T), a substantial contribution to the signal change was made by noncapillary vessels.

DISCUSSION

The field of functional brain mapping by MRI is now rapidly growing. Experiments similar to that shown in Fig. 1, but with reduced fractional signal change to noise ratio, have even been demonstrated at 1.5 T, the field strength used in present clinical scanners. Although echo-planar fast imaging may be preferable to reduce motion artifacts and have increased temporal resolution, successful images have been achieved with a regular fast low angle shot pulse sequence (22). Although the method depends on similar hemodynamic responses to neural activation that PET measurements do, the spatial resolution of the functional mapping is higher with MRI, and high-resolution anatomical images can be obtained in the same imaging session, so that registration of functional maps with defined anatomical structures is possible. The measurement is completely noninvasive and can be repeated on the same subject many times, so that averaging, where necessary, can be done on a single subject and the problems of averaging with intersubject variability eliminated. The MRI imaging method has a relatively slow time resolution (a repetition time in the order of seconds), but this is the same order as the hemodynamic response times (2, 3), and it is higher than that demonstrated with PET imaging.

The principal effect observed in gradient echo images of primary sensory cortex is a sustained change in the signal intensity during sensory stimulation. However, as shown in Fig. 2, superimposed on this sustained signal change is a reproducible oscillatory dynamics. So far, oscillations of this form have been reported only for experiments at high field, where the fractional signal changes $\Delta S/S$ are large and the spatial resolution is higher. It is unclear if they have a neural origin, i.e., the neural activity induced by the sensory stimulation has a slow periodicity and the time course of hemodynamics simply follows the neural activity pattern. An alternative hypothesis is that the hemodynamic response itself has this time dependence for a constant level of neural activity. If the oscillations represent a neural origin, then it may be possible to measure spatial correlations of the responses across the cortex. This would provide an MRI

method of mapping patterns of functional connections between cortical areas.

The signal characteristics of BOLD-based MRI need to be explained in biophysical terms. Most experiments at 4 T have shown large fractional increases in signal intensity $\Delta S/S$ of 5–20% in the primary cortical areas for the corresponding sensory stimulation. Smaller fractional increases (1–3%) have been observed at 1.5 T. This result suggests a superlinear increase in fractional change with field strength. Our numerical simulations were primarily designed to see if our present understanding of the biophysical basis of BOLD imaging can account for the amplitude, sign, and field dependence of the signal change. Simulations were performed in a parameter appropriate for human brain imaging experiments at 1–4 T. A related goal was to determine in a more quantitative way how changes in physiological parameters such as CBF, CBV, oxygen extraction (o.e.), and the size distribution and spatial distribution of active vessels affect BOLD contrast.

The BOLD signal change depends on the changes in fractional blood oxygenation Y. Y itself depends on the oxygen extraction (o.e.) (moles O_2/(gram tissue) seconds) and the CBF (milliliters of blood/(gram tissue) seconds). The relationship is dictated by Fick's principle:

$$(\text{o.e.}) = CBF\,[\text{Hemoglobin}]\,(1 - Y),$$

where [Hemoglobin] is the ferrous heme concentration in blood, moles per milliliter of blood. In terms of the changes in these hemodynamic parameters, the above relation of the arteriovenous oxygen balance is

$$1 + \Delta(\text{o.e.})/(\text{o.e.})$$
$$= (1 + \Delta CBF/CBF)(1 - \Delta Y/(1 - Y)). \quad (6)$$

This expression shows that the change in Y that is appropriate to determine the magnitude of the BOLD effect depends on both the fractional change in CBF and the change in oxygen extraction. PET experiments that examined changes in cerebral cortical hemodynamics produced by sensory stimulation have concluded that there is little change in oxygen extraction produced ($\Delta(\text{o.e.})/$ (o.e.) ~ 0). This would imply from Eq. 6 that a fractional increase in CBF would be directly reflected in a corresponding fractional increase of Y, simplifying somewhat the interpretation of BOLD image changes.

It is important to note that even the sign of the change in BOLD signal produced by a change in neural activation depends on the specific kind of hemodynamic response. It is generally accepted that neural activation is accompanied by an increase in CBV and CBF. For example, using paramagnetic contrast agents, Belliveau et al. (23) reported the change of CBV in visual cortex induced by photic stimulation. As previously mentioned, there is still some uncertainty over the issue of whether or not there is an increase of oxygen extraction. As shown in Eq. 5, an increase in CBV without any change in Y will produce a reduction in the signal intensity, regardless of whether one is talking about the recruitment or swelling model, basically because this means that this corresponds to a local increase of the concentration of paramagnetic contrast agent and thus more intravoxel dephasing. But this effect can be reduced and even reversed by an increase in Y, such as that produced by a large increase in CBF. Qualitatively, sufficiently large increases in venous blood oxygenation can reduce the effective concentration of paramagnetic contrast agent even though the fractional blood volume has increased.

In all visual cortex photic stimulation experiments we have performed and also in the results reported by others, the gradient echo signal intensity increases with sensory stimulation. This must mean that the effects on BOLD of increased oxygenation have reversed the effects expected from an increase in CBV. PET imaging experiments suggested that there would be an increase in venous blood oxygenation. The MRI results go further to suggest that the large CBF increase induces a sufficiently large increase in Y and that it can produce an increase in BOLD signal despite the increase in CBV.

The sign of the BOLD-based signal change may not always be positive. It is possible that differences in basal physiological states, intersubject differences, and differences in the cerebral hemodynamic responses between different brain areas may be large and have not been sampled adequately in previous PET and MRI experiments. We have observed in BOLD imaging experiments near cortical motor areas that finger motion produces strong positive signal changes in some cortical areas and strong negative changes in other nearby areas (24). Similar results recently have been obtained in optical reflection imaging experiments from the cortex of neurosurgical patients (8). Further work is necessary to understand the origin and meaning of this effect.

In addition to the qualitative interpretation of our results provided above, the expressions we have provided for R_2^* can, with the estimates of CBF and CBV changes provided by PET measurements and some reasonable assumptions, be used to provide a quantitative estimate the stimulation induced signal changes ($\Delta S/S = -t_{echo}\Delta R_2^*$) that have been observed at 4 T (19) in photic stimulation experiments. If we assume initial blood volume fractions of $b_l = 0.01$ and $b_s = 0.03$ for noncapillary and capillary, respectively, $\Delta CBF/CBF = 0.75$ with $Y = 0.6$, $\Delta \text{o.e.}/\text{o.e.} = 0$, and $\Delta CBV/CBV = 0.2$ with equal fractional changes in the large and small vessels, then Eq. 5 predicts a fractional signal increase of $\Delta S/S = 8\%$ at 4 T (echo time $t_e = 40$ ms; $\alpha = 4.3$ and $\beta = 0.04$ in Eq. 5). This compares reasonably well with the observed changes of 5–20%.

To optimize BOLD imaging, it is important to determine how the signal change depends on the applied magnetic field strength. Reported values of $\Delta S/S$ at 4 T seem to be larger than the values at 1.5 T by more than the

field strength ratio of 2.7. The field strength dependence of $\Delta S/S$ implied in Eq. 5 depend on the relative contributions capillary and noncapillary venous blood vessels, but the capillary contribution has a ν^2 dependence. The estimated value of $\Delta S/S$ for 1.5 T field in the above estimate using the same Eq. 5 is 0.016. Thus, the simplified picture presented by our numerical simulations would be consistent with the field dependence observed experimentally if the capillary contribution contributes significantly at high field. Note that at low magnetic field strength, the capillary (second term) contribution may be less important because the ΔR_2^* from this term is small at the low value of ν (see Fig. 3).

The ν^2 dependence for capillaries that is suggested from the results of our numerical simulations is different from that suggested by other analysis and experiments. At very high values of ν, like those produced by exogenous paramagnetic vascular contrast agents (e.g., gadolinium diethylenetriamine pentaacetic acid), numerical calculations have suggested that the signal change is linear to the ν value (25) or concentration of the contrast agent, a result that was important in relating observed signal changes to a quantitative estimate of regional CBV. In a study of the sensitivity of the BOLD-based signal amplitude to venous blood oxygenation at high field (7 T), Ogawa et al. (9) observed a rather linear relation between R_2^* and the ν value in rat cortical areas. These results at high ν are not necessarily inconsistent with our numerical results. As shown in Fig. 5, the R_2^* value for capillary bed at very high ν values does not increase in ν^2 but nearly linear. However, since the assumption of no intercapillary interaction for the local fields may not be applicable to these cases of high ν value, a different approach for numerical simulation may be required.

Compared with the complex nature of the BOLD-based signal change discussed above, direct MRI measurements of CBF, for example using inversion-recovery methods, have the advantage that the observed changes can be quantified more easily. However, the expected and measured signal changes are small. For example, Kwong et al. (2) reported a stimulation produced signal change of 2% in inversion-recovery measurements of proton (blood water) perfusion in primary cerebral cortex. Nevertheless, the perfusion measurement is essentially magnetic field strength independent and may be useful in functional mapping in low field instruments such as present clinical scanners (1.5 T).

BOLD-based functional brain mapping is being pursued in many laboratories worldwide. Although most of the experimental results that have been reported deal with sensory stimulation experiments, attempts to map brain areas involved in higher cognitive functions such as mental imagery are being actively pursued. Even without a quantitative understanding of how observed signal changes correspond to hemodynamic variables, the technique can provide maps of brain areas that show altered activity in human mental operations. However, a quantitative biophysical picture of the nature of the signal change such as we have been pursuing here will no doubt be valuable in the development of MRI-based functional brain mapping. Our results were based on a very simple model of cerebral vasculature and hemodynamic change. A more accurate picture will require the use of realistic vessel populations and geometry, and effects that result from the interactions of water molecules with multiple vessels may have to be included. It seems likely that a detailed, large-scale numerical analysis will be required to provide results of a biophysical model that can be quantitatively compared with specific experiments.

REFERENCES

1. Ogawa, S., D. W. Tank, R. Menon, J. M. Ellermann, S.-G. Kim, H. Merkle, and K. Ugurbil. 1992. Intrinsic signal changes accompanying sensory stimulation: functional brain mapping with magnetic resonance imaging. *Proc. Natl. Acad. Sci. USA.* 89:5951–5955.

2. Kwong, K. K., J. W. Belliveau, D. A. Chesler, E. I. Goldberg, R. M. Weisskoff, B. P. Poncelet, D. N. Kennedy, B. E. Hoppel, M. S. Cohen, R. Turner, H. M. Cheng, T. J. Brady, and B. R. Rosen. 1992. Dynamic magnetic resonance imaging of human brain activity during primary sensory stimulation. *Proc. Natl. Acad. Sci. USA* 89:5675–5679.

3. Bandettini, P. A., E. C. Wong, R. S. Hinks, R. S. Tikofsky, and J. S. Hyde. 1992. Time course EPI of human brain function during task activation. *Magn. Reson. Med.* 25:390–397.

4. Fox, P. T., and M. E. Raichle. 1986. Focal physiological uncoupling of cerebral blood flow and oxidative metabolism during somatosensory stimulation in human subjects. *Proc. Natl. Acad. Sci. USA.* 83:1140–1144.

5. Fox, P. T., M. E. Raichle, M. A. Mintun, and C. Dence. 1988. Nonoxidative glucose consumption during focal physiologic neural activity. *Science (Wash. DC).* 241:462–464.

6. Frostig, R. D., E. E. Lieke, D. Y. Ts'o, and A. Grinvald. 1990. Cortical functional architecture and local coupling between neuronal activity and the microcirculation revealed by in vivo high-resolution optical imaging of intrinsic signals. *Proc. Natl. Acad. Sci. USA.* 87:6082–6086.

7. Grinvald, A., R. D. Frostig, R. M. Siegel, and R. M. Bartfeld. 1991. High-resolution optical imaging of functional brain architecture in the awake monkey. *Proc. Natl. Acad. Sci. USA.* 88:11559–11563.

8. Haglund, M. M., G. A. Ojemmann, and D. W. Hochman. 1992. Optical imaging of epileptiform and functional activity in human cerebral cortex. *Nature (Lond.).* 358:668–671.

9. Ogawa, S., T. M. Lee, and B. Barrere. 1993. Sensitivity of magnetic resonance image signals of a rat brain to changes in the cerebral venous blood oxygenation. *Magn. Reson. Med.* In press.

10. Ogawa, S., T. M. Lee, A. S. Nayak, and P. Glynn. 1990. Oxygenation-sensitive contrast in magnetic resonance image of rodent brain at high fields. *Magn. Reson. Med.* 14:68–78.

11. Ogawa, S., T. M. Lee, A. R. Kay, and D. W. Tank. 1990. Brain magnetic resonance imaging with contrast dependent on blood oxygenation. *Proc. Natl. Acad. Sci. USA.* 87:9868–9872.

12. Pauling, L., and C. D. Coryell. 1936. The magnetic properties and

structure of hemoglobin, oxyhemoglobin and carbonmonoxy-hemoglobin. *Proc. Natl. Acad. Sci. USA.* 22:210–216.

13. Reilly, C. A., H. M. McConnell, and R. G. Meisenheimer. 1955. Nuclear magnetic resonance spectra of annular samples. *Phys. Rev.* 98:264a. (Abstr.)

14. Fisel, C. R., J. L. Ackerman, R. B. Buxton, L. Garrido, J. W. Belliveau, B. R. Rosen, and T. J. Brady. 1991. MR contrast due to microscopically heterogeneous magnetic susceptibility: numerical simulations and applications to cerebral physiology. *Magn. Reson. Med.* 17:336–347.

15. Hardy, P., and R. M. Henkelmen. 1991. On the transverse relaxation rate enhancement induced by Diffusion of Spins through inhomogeneous fields. *Magn. Reson. Med.* 17:348–356.

16. Springer, C. S., and Y. Xu. (1991). Aspects of bulk magnetic susceptibility in in vivo MRI and MRS. New developments in contrast agent research. P. A. Rinck and R. N. Muller, editors. European Magnetic Resonance Forum, Blonay, Switzerland. 13–25.

17. Ogawa, S., and T. M. Lee. 1990. Magnetic resonance imaging of blood vessels at high fields: in vivo and in vitro measurements and image simulation. *Magn. Reson. Med.* 16:9–18.

18. Pawlik, G., A. Rackl, and R. J. Bing. 1981. Quantitative capillary tropography and blood flow in the cerebral cortex of cats: an in vivo microscopic study. *Brain Res.* 208:35–58.

19. Menon, R., S. Ogawa, S.-G. Kim, H. Merkle, D. W. Tank, and K. Ugurbil. 1992. Functional brain imaging: 4 Tesla echo time dependence of photic stimulation induced signal changes in the human primary visual cortex. Society of Magnetic Resonance in Medicine. 11th Annual Meeting, Berlin, Germany. p.1852.

20. Le Bihan, D. L., and R. Turner. 1991. Intravoxel incoherent motion imaging using spin echoes. *Magn. Reson. Med.* 19:221–227.

21. Bandettini, P. A., E. C. Wong, R. S. Hinks, I. Estkowski, and J. S. Hyde. 1992. Quantification of changes in relaxation rates R2* and R2 in activated brain tissue. Society of Magnetic Resonance in Medicine. 11th Annual Meeting, Berlin, Germany. p.719.

22. Frahm, J., H. Bruhn, K.-D. Merboldt, W. Hanicke, and D. Math. 1992. Dynamic MRI of human brain oxygenation during rest and photic stimulation. *J. Magn. Reson. Imaging.* 2:501.

23. Belliveau, J. W., D. N. Kennedy, R. C. McKinstry, B. R. Buchbinder, R. M. Weisskoff, M. S. Cohen, J. M. Vevea, T. J. Brady, and B. R. Rosen. 1991. Functional mapping of the human visual cortex using magnetic resonance imaging. *Science (Wash. DC).* 254:716–719.

24. Kim, S.-G., H. Merkle, J. Ashe, A. Georgopoulos, R. Menon, J. Ellermann, S. Ogawa, D. W. Tank, and K. Ugurbil. 1992. Functional mapping of human motor cortex at high magnetic field. Society of Magnetic Resonance in Medicine. 11th Annual Meeting, Berlin, Germany. p.1825.

25. Rosen, B. R., J. W. Belliveau, J. M. Vevea, and T. J. Brady. 1990. Perfusion imaging with NMR contrast agents. *Magn. Reson. Med.* 14:249–265.